Applied Catalysis B: Environmental 132–133 (2013) 342–352

Contents lists available at SciVerse ScienceDirect

Applied Catalysis B: Environmental

journal homepage: www.elsevier.com/locate/apcatb

Catalytic wet air oxidation of bisphenol A model solution in a trickle-bed reactor over titanate nanotube-based catalysts

Boštjan Erjavec[a,b,*], Renata Kaplan[a], Petar Djinović[a,b], Albin Pintar[a,b]

[a] Laboratory for Environmental Sciences and Engineering, National Institute of Chemistry, Hajdrihova 19, SI-1001 Ljubljana, Slovenia
[b] Center of Excellence "Low Carbon Technologies", Hajdrihova 19, SI-1001 Ljubljana, Slovenia

ARTICLE INFO

Article history:
Received 18 July 2012
Received in revised form 3 December 2012
Accepted 7 December 2012
Available online 16 December 2012

Keywords:
Catalytic wet air oxidation
Bisphenol A
TiO_2
Water treatment
Titanate nanotubes
Hydrothermal synthesis

ABSTRACT

Titanate nanotube-based catalysts were prepared via alkaline hydrothermal synthesis route followed by heat-treatment at different temperatures, ranging from 300 to 700 °C. The resulting metal-free solids were then applied as a catalyst in a three-phase trickle-bed reactor, where catalytic wet air oxidation (CWAO) reactions of model aqueous bisphenol A (BPA) solution were performed. Mainly, the CWAO experiments were conducted at 200 °C with oxygen partial pressure of 10 bar over 300 mg of a catalyst. It was observed in the given range of operating conditions that BPA undergoes both non-catalytic as well as catalytic oxidation routes, while the latter is far more pronounced. At 210 °C and in the presence of 0.5 g of titanate nanotube-based catalyst, which was annealed at 600 °C, complete BPA removal was obtained. From TOC point of view, approximately 70% conversion was achieved indicating the persistence of refractory intermediates of lower carboxylic acids. The cross-section of results derived from various analytical techniques, which were used to identify surface, textural and morphological properties, revealed that balanced physicochemical properties are required to achieve meaningful extent of BPA removal. During 2–4 day time on stream, no catalyst deactivation occurred that could be attributed to the dissolution of active powders, or to the carbonaceous deposits accumulated on the catalyst surface. Therefore, these nanotubular materials can be regarded as innocuous and efficient long-term catalysts for oxidation of hazardous organic compounds (such as BPA) in the CWAO process.

1. Introduction

Bisphenol A (BPA) is widely used by the manufacturers as an intermediate in the production of polycarbonate and epoxy resins, flame retardants and other special products [1]. Because of its extensive usage and its endocrine disrupting effects, BPA is regarded as a representative material among endocrine disrupting compounds (EDCs) and acts adversely to aquatic organisms [2–4]. Reports show that the contamination routes of BPA in the aquatic environment mainly originate from wastewater treatment plants and landfill leachates [5]. EDCs present in drinking water supplies may also pose a threat to human population as an increase of hormone related cancers have been often attributed to EDCs [6]. Therefore, in the last decade, there is an increasing interest in effective remediation technologies for the destruction of BPA in contaminated water environments.

Conventional biological methods to treat emerging organic pollutants in wastewaters require long residence times, since these processes are based on activated sludge and/or carbon adsorption systems, which are inefficient in removing and degrading various phenolic EDCs including BPA and alkylphenols [7,8]. Furthermore, a large part of EDCs are in fact removed by adsorption onto activated sludge, which can cause further problems in sludge management [9,10]. If the sludge is discarded over soil, the pollutant could remain in the soil for a long time due to the sorption and slow rate of biodegradation [11]. The biodegradation efficiency is affected by the initial concentration of target pollutants, which are also the substrates of the enzyme (produced by microorganisms) reactions. Accordingly to the Michaelis–Menten kinetics, certain amount of BPA is necessary to achieve good biodegradation efficiency. Therefore, low concentrations of BPA are difficult to be effectively degraded in ordinary wastewater treatment plants. For example, 0.542 mg l^{-1} BPA was degraded to 0.162 mg l^{-1}, while 3.01 mg l^{-1} BPA was reduced to 0.258 mg l^{-1} in a wastewater treatment plant in Germany, resulting in removal efficiency of 70 and 91%, respectively [12]. In addition, the degradation of BPA at low concentrations usually requires a long incubation time and sometimes includes a lag phase. For example, biodegradation half-lives for BPA were 0.5–3 days at the initial concentrations

* Corresponding author at: Laboratory for Environmental Sciences and Engineering, National Institute of Chemistry, Hajdrihova 19, SI-1001 Ljubljana, Slovenia. Tel.: +386 1 47 60 470; fax: +386 1 47 60 460.
E-mail address: bostjan.erjavec@ki.si (B. Erjavec).

0926-3373/$ – see front matter © 2012 Elsevier B.V. All rights reserved.
http://dx.doi.org/10.1016/j.apcatb.2012.12.007

of 50–5500 $\mu g\,l^{-1}$, but 3–6 days at environmentally relevant concentrations (0.05–0.5 $\mu g\,l^{-1}$) with lag phases of 2–4 days, using sediment and water collected from rivers [13]. To increase the biodegradation efficiency, systems including membrane bioreactors or biomass immobilization have been lately developed [14]. Therefore, new techniques that can effectively degrade BPA at low concentrations, are in great need.

The effective removal of BPA is usually limited to advanced oxidation processes (AOPs), such as catalytic wet air oxidation, heterogeneous photocatalysis, Fenton oxidation, ozonation and ultrasound oxidation [15–19]. In general, purifying techniques available for treating hazardous organic pollutants in aqueous solutions are very diverse and frequently one or more treatment techniques in sequence or parallel are required to completely degrade these compounds. However, catalytic wet air oxidation (CWAO) process is regarded as one of the most promising AOP solutions for achieving meaningful extent of mineralization (i.e., transformation into CO_2 and H_2O) of evolving organic contaminants. In comparison to the wet air oxidation (WAO) process, where large energy inputs (i.e., high pressure and temperature) are required, the CWAO process can be efficiently conducted under milder operating conditions, due to the performance of heterogeneous catalysts. Therefore, typical CWAO temperatures and pressures are between 130–250 °C and 10–50 bar, respectively. Depending on the type and amount of organic compounds dissolved in wastewater (WW), the process can be designed in a way to completely oxidize these pollutants by activated O_2 species (via free radical mechanism) to innocuous inorganic compounds [20,21].

Selection of the proper catalyst for CWAO process not only diminishes the severity of reaction conditions, but also enhances the decomposition of refractory organic pollutants, thereby reducing investment and operational cost [22,23]. In general, the homogenous catalysts, e.g., dissolved copper salts, are regarded as effective, but an additional separation step is needed for removal or recovery of metal ions from the treated effluent due to their toxicity, which substantially increases operational costs. Hence, the development of active heterogeneous catalysts has received great attention because a separation step is not obligatory. Concerning the activity of catalysts, extent of mineralization of hazardous organic pollutants as well as life time under hydrothermal operating conditions, supported noble metal catalysts, such as Ru, Rh, Pd, Ir and Pt, have proved to be the most efficient. In addition, supported mixed metal oxides of Cr, Mn, Fe, Co, Ni, Cu, Zn, Mo and Ce are also recognized as competent catalysts in CWAO processes [21]. Unfortunately, these metal oxides are often subjected to leaching and thus deteriorate the quality of treated waters, while the catalysts based on noble metals sharply increase the investment cost. Generally, the active metals are supported on TiO_2, ZrO_2, CeO_2, γ-Al_2O_3 and carbon materials with less than 5% of metal loading [24]. Particularly TiO_2 is often applied to support noble metals; however, there is very scarce literature available regarding self-dependent TiO_2 catalysts in CWAO process. Pintar et al. [25] reported TOC conversions vs. reaction temperature dependencies obtained during the oxidation of aqueous phenol solution in the presence of Ru/TiO_2 catalyst and bare TiO_2 support, respectively. Interestingly, the bare TiO_2 support exhibited catalytic activity under oxidizing conditions at temperatures higher than 160 °C (e.g., 40% TOC removal at 240 °C). Examination of spent TiO_2 support using XRD and TC analyses showed intact crystal structure without carbonaceous deposits on the surface. Yang et al. [26] obtained about 15% COD conversion in the CWAO of phenol over pure TiO_2. Furthermore, poor catalytic activity in the CWAO of acetic acid, which is a refractory organic compound, was spotted over pure TiO_2 and CeO_2 catalysts [27]. The former degraded 9% of acetic acid, while the later oxidized 14% of organic compound at 230 °C and 5 MPa after 180 min of reaction time in a batch reactor. Since TiO_2 bears characteristics like insolubility, resistance to corrosion, very low toxicity, inexpensiveness, and after all exhibits a moderate catalytic activity in the CWAO processes, it can be regarded as an advantageous catalyst candidate.

Recently, nanostructured one-dimensional (1D) titanates such as nanotubes (NTs), nanoribbons and nanowires have attracted a lot of attention due to their unique physicochemical properties and improved performance in various applications [28]. Among 1D titanate nanostructures, titanate nanotubes possess high specific surface area nanotubular morphology, which facilitates the catalytic reaction. Most of the catalytic studies of titanate nanotubes are, however, focused on the utilization of its surface as a support for highly dispersed catalysts [29]. TiO_2-based nanotubes, more precisely titanate nanotubes are in general synthesized by three different approaches: (i) the chemical (template assisted) method [30], (ii) electrochemical anodic oxidation [31] and (iii) alkaline hydrothermal method [32]. Among these methods, hydrothermal treatment has attracted the most attention due to its cost-effectiveness and simplicity [33]. Heat-treatment of titanate nanotubes at different temperatures can yield products with diverse crystal-phase compositions, morphologies, pore structures and surface properties [34]; consequently, there is a great interest to understand how catalytic activity of annealed (at different temperatures) titanate-based solids in the CWAO process varies with substantial changes.

In the present study, protonated titanate nanotubes with specific surface area approaching 400 $m^2\,g^{-1}$ were synthesized under various hydrothermal reaction conditions. The subsequent heat-treatment of the selected nanotubular sample at different temperatures resulted in titanate nanotube-based catalysts with various catalytic properties. Hereafter, we report a novel approach to destruction of estrogenic active organic compounds in the CWAO process over pure high specific surface area titanate nanotubes (without surface decoration with active metals). The CWAO of BPA model aqueous solutions was carried out in a continuous-flow trickle-bed reactor in order to investigate a potential of bare titanate nanotube-based catalyst for effective (i.e., long-term) removal of the parent molecule and possible intermediates from the liquid phase. The feed and end-product solutions were analyzed by means of HPLC, TOC and UV–vis techniques, in order to examine global efficiencies of investigated catalysts for degradation of BPA dissolved in water. The textural, surface and morphological properties of tested catalysts were investigated using TEM, SEM, XRD, UV–vis–DRS, FT-IR, TG and BET analytical techniques. The CHNS elemental analysis of fresh and spent catalysts was applied to evaluate the amount of carbonaceous deposits accumulated during the CWAO experiments, with a view to estimate whether catalysts based on titanate nanotubes were suitable for a long-term purification of polluted water in the CWAO process.

2. Experimental

2.1. Synthesis of titanate NTs

TiO_2-based NTs were synthesized using a similar procedure to that reported by Kasuga et al. [32]. TiO_2 powder (P25, Degussa AG) was dispersed in 10 M NaOH solution by means of ultrasonic homogenizer. A teflon-lined autoclave was then filled with the reaction mixture up to 75% of its volume and held at 130 °C for at least 24 h. Several synthesis conditions were varied (Table 1) in order to obtain morphologic homogeneity of high surface area nanotubular TiO_2 samples. The resulting white precipitates were separated from reaction solution by filtration process, followed by thorough rinsing with deionized water. In the subsequent step,

Table 1
Hydrothermal synthesis conditions of various samples prepared in this study.

Sample	$m_{P25\ Degussa}$ (g)	V_{NaOH} (ml)	$t_{react.}$ (h)	$T_{react.}$ (°C)	P_{Ar} (bar)[a]
NT1	1.0	150	24	130	–
NT2	1.0	150	24	130	25
NT3	1.0	150	48	130	–
NT4	2.0	150	24	130	–
NT5	0.5	150	24	130	–

[a] Pressure of imposed inert gas (Ar).

the wet cakes were dispersed into 500 ml of 0.1 M HCl solution and kept under ambient conditions for 24 h, in order to promote proton exchange mechanism. The whole HCl treatment process was repeated three times, each day with a fresh 0.1 M HCl solution, followed by neutralization with deionized water. Finally, the samples were dried in vacuum under cryogenic conditions, removing adsorbed water without altering the structure of the synthesized materials.

2.2. Titanate nanotube-based catalyst preparation

On the basis of preliminary characterization of NTs prepared by hydrothermal synthesis, a restriction to only one NT sample was made. The selected sample was then heat-treated at 300, 400, 500, 600, and 700 °C for 1 h in air, in order to vary particle size, crystal structure, morphology and surface properties.

2.3. Characterization of NTs and titanate nanotube-based catalysts

The selection of NTs was made by means of two distinguished characterization techniques. The surface morphology of the synthesized materials was examined by field-emission scanning electron microscope (FE-SEM SUPRA 35VP, Carl Zeiss). For TEM investigations, the materials were deposited on a copper-grid-supported perforated transparent carbon foil. A field-emission electron-source transmission electron microscope (JEOL 2010 F) was used. Specific surface area, total pore volume and average pore width of the NTs were determined from the adsorption and desorption isotherms of N_2 at −196 °C using a Micromeritics TriStar II 3020 instrument. This characterization was performed after gradual degassing of samples under a N_2 stream (purity 6.0) and programmed bi-level heating, starting with the first heating stage at 90 °C for 60 min and followed by the second heating stage at 180 °C for 240 min. The heating rate was set to 10 °C min^{-1} for both heating stages. The specific surface area of the samples was calculated by applying the BET theory to the nitrogen adsorption data within the 0.06–0.30 p/p^0 range. Pore-size distributions were calculated from the desorption branch of the corresponding nitrogen isotherm, employing the BJH method.

The dehydration process of the as-prepared protonated titanate nanotubes was monitored using TPO/TGA analysis (Pyris 1 by Perkin-Elmer). After annealing the favoured sample at temperatures up to 700 °C, dissimilar titanate nanotube-based catalysts were obtained. Their surface morphology, specific surface area, total pore volume and average pore width were examined and determined, using the same apparatus as mentioned above. The X-ray powder diffraction patterns of the catalysts were collected on PANalytical X'pert PRO MPD diffractometer using Cu Kα1 radiation (1.54056 Å) in reflection geometry. The data were collected in the range between 10° and 90° in steps of 0.034°. Crystalline phases were identified by comparison with PDF standards from the International Centre for Diffraction Data (ICDD).

Diffuse reflectance UV–vis spectra of heat-treated titanate nanotube-based catalysts as well as of reference materials were recorded at room temperature using a Perkin-Elmer Lambda 35 UV-Vis spectrophotometer equipped with the RSA-PE-19M Praying Mantis accessory, which is designed for diffuse reflectance measurements of horizontally positioned powder samples, pastes or rough surface samples. The Spectralon® white reflectance standard was used to perform the instrument background correction in the range of 200–900 nm. The scans were acquired with speed of 120 nm min^{-1} and slit set to 4 nm. FT-IR spectra were recorded in the range of 400–4000 cm^{-1} using a FT-IR analyzer model Frontier 100 (Perkin-Elmer), equipped with GladiATR Vision™ (PIKE Technologies) accessory that contained a diamond crystal.

The carbon content of fresh and spent titanate nanotube-based catalysts was determined by CHNS analyzer (Perkin-Elmer, model 2400 Series II), in order to evaluate the amount of accumulated carbonaceous deposits on the catalysts surface.

Table 2
Operating conditions of a continuous-flow trickle-bed reactor during CWAO experiments.

Mass of catalyst in bed (g)	0.3, 0.5
Bed density (g cm^{-3})	0.11
Reaction temperature (°C)	200, [a]210
Total operating pressure (bar)	25.5, [a]29.1
Oxygen partial pressure (bar)	10.0
Gas flow rate (ml min^{-1})	60
Superficial gas flow rate (kg m^{-2} s^{-1})	0.357, [a]0.399
Liquid flow rate (ml min^{-1})	0.5
Superficial liquid flow rate (kg m^{-2} s^{-1})	0.134, [a]0.133
BPA concentration (mg l^{-1})	10

[a] T = 210 °C.

2.4. Catalytic experiments

Catalytic wet air oxidation (CWAO) experiments were performed in a Microactivity-Reference unit (PID Eng&Tech, Spain), which is a fully automated and computer-controlled, continuous-flow trickle-bed reactor for catalytic tests. A cardinal part of the unit, where a water-dissolved pollutant was oxidized, was a tubular reactor (Autoclave Engineers, USA), made of a 305 mm (l.) × 9 mm (i.d.) Hastelloy C-276 tube. The aqueous feed solution with the BPA concentration of 10.0 mg l^{-1} (min. 99%, Aldrich) was introduced into the reactor unit by HPLC positive alternative displacement pump (Gilson, model 307). The oxygen source in these experiments was pure O_2 (purity 5.0, Messer), which was fed into the system through an electronic HI-TEC mass-flow controller (Bronkhorst, model EL-FLOW). A detailed description of the apparatus can be found elsewhere [25]. It should be noted that a typical continuous-flow CWAO test lasted for 40 h, taking into account the time period of approximately 20 h needed to establish dynamic equilibrium between phases in the catalyst layer. After initial non-equilibrium, a steady-state performance was obtained giving rise to good reproducibility of oxidation capacity. The properties of the catalyst bed and operating conditions are listed in Table 2.

Representative liquid-phase samples were continuously collected from the L/G condenser/separator during the CWAO experiments by microcomputer controlled fraction collector (ADVANTEC®, model CHF122SC) and further analyzed for residual BPA content using HPLC analysis and UV–vis spectroscopy. Determinations performed by HPLC apparatus (Spectra system™) were carried out in the isocratic analytical mode using a 100 mm × 4.6 mm BDS Hypersil C18 2.4 μm column thermostated at 30 °C and equipped with an universal column protection system (UV detection at λ = 210 nm with a mobile phase of methanol (70%) and ultrapure water (30%) at a flow rate of 0.5 ml min^{-1}). Additionally, a Perkin-Elmer (model Lambda 45) UV-Vis spectrophotometer combined with a 8-cell manual changer was used to determine the residual concentrations of BPA in the aqueous-phase samples. The composition of collected liquid-phase samples was additionally analyzed by ion chromatography (IC) using DX-120

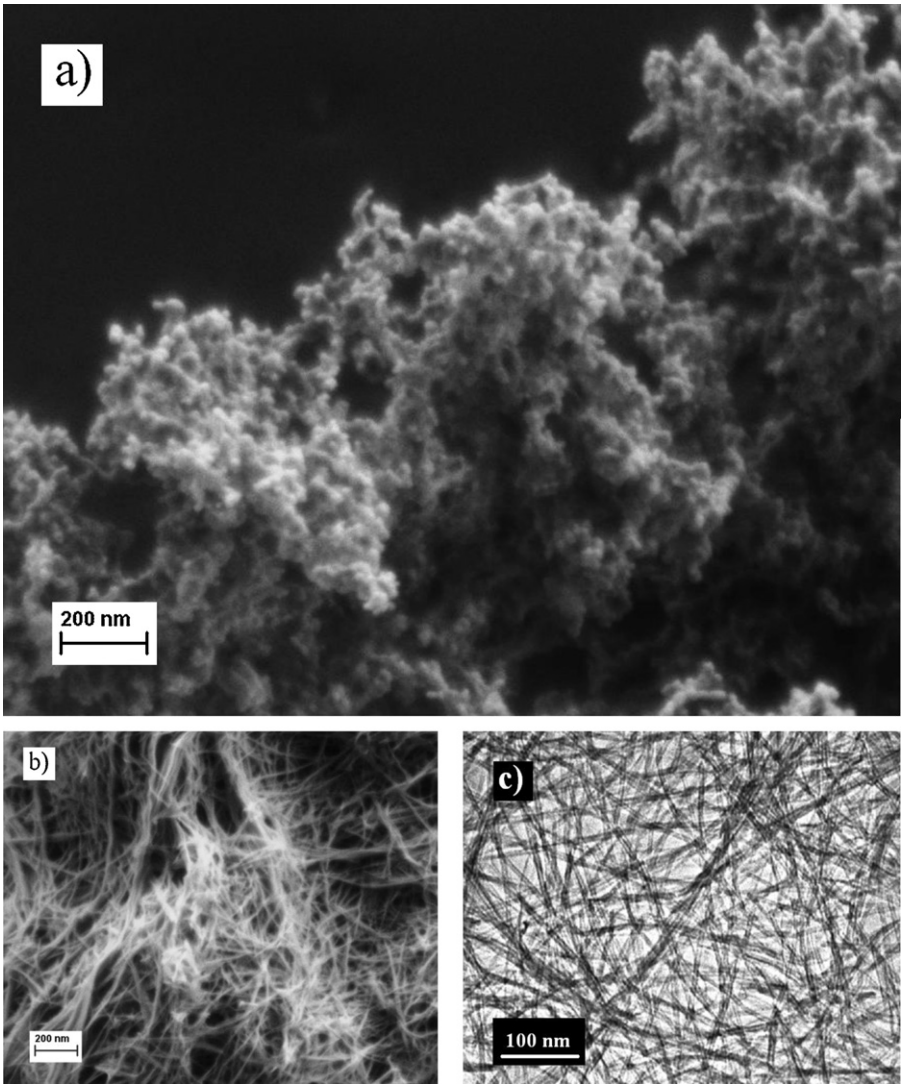

Fig. 1. SEM micrographs of (a) precursor material (P25 Degussa) and (b) as-prepared titanate nanotubes (NT4). (c) TEM micrograph of as-prepared titanate nanotubes (NT4).

Dionex apparatus, in order to determine eventual CWAO intermediates.

The level of mineralization, i.e., the total amount of removed organic substances in withdrawn aqueous-phase samples, was determined by measuring the total organic carbon (TOC). TOC content measurements were carried out with an advanced TOC analyzer (Teledyne Tekmar, model Torch) equipped with a high-pressure NDIR detector. A high-temperature catalytic oxidation (HTCO) method was applied (at 750 °C), which subtracted the measured inorganic carbon (IC) content from measured total carbon (TC) content. In all analyses, 2–3 repeated measurements were taken for each liquid-phase sample, and the average value of TOC concentration was reported.

Leaching of Ti from catalysts during the CWAO reaction was verified by inductively coupled plasma atomic emission spectrometer (ICP-AES; Thermo Jarrell Ash, model Atomscan 25) of collected liquid-phase samples.

3. Results and discussion

3.1. Characterization of NTs

Table 3 summarizes the BET surface area, total pore volume and average pore width of the as-prepared NT samples and precursor material P25 Degussa. The former possess the specific surface areas ranging roughly from 300 to 400 $m^2\ g^{-1}$, while the thoroughly explored P25 Degussa sample exhibits the expected BET surface area of 52 $m^2\ g^{-1}$. These first observations are in accordance with the research work done by Tsai and Teng [35] and Kasuga et al. [32], where the highest obtainable BET surface areas of nanotubular titania materials are stated to reach 400 $m^2\ g^{-1}$.

A closer look at Table 1 reveals that while preparing samples NT1, NT4 and NT5, the weight of precursor P25 Degussa powder was the only variable that was varied (the NaOH solution volume, reaction time and reaction temperature remained fixed). The synthesis results are clearly discernible in Table 3, where the trends

Table 3
Specific surface area (S_{BET}), total pore volume (V_{pore}) and average pore width (d_{pore}) of precursor material (P25 Degussa) and various nanotubular materials obtained via alkaline hydrothermal synthesis.

Sample	S_{BET} ($m^2\ g^{-1}$)	V_{pore} ($cm^3\ g^{-1}$)	d_{pore} (Å)
NT1	339	1.30	140
NT2	366	1.70	167
NT3	392	1.74	159
NT4	383	1.60	149
NT5	303	0.74	87
P25 Degussa	52	0.15	102

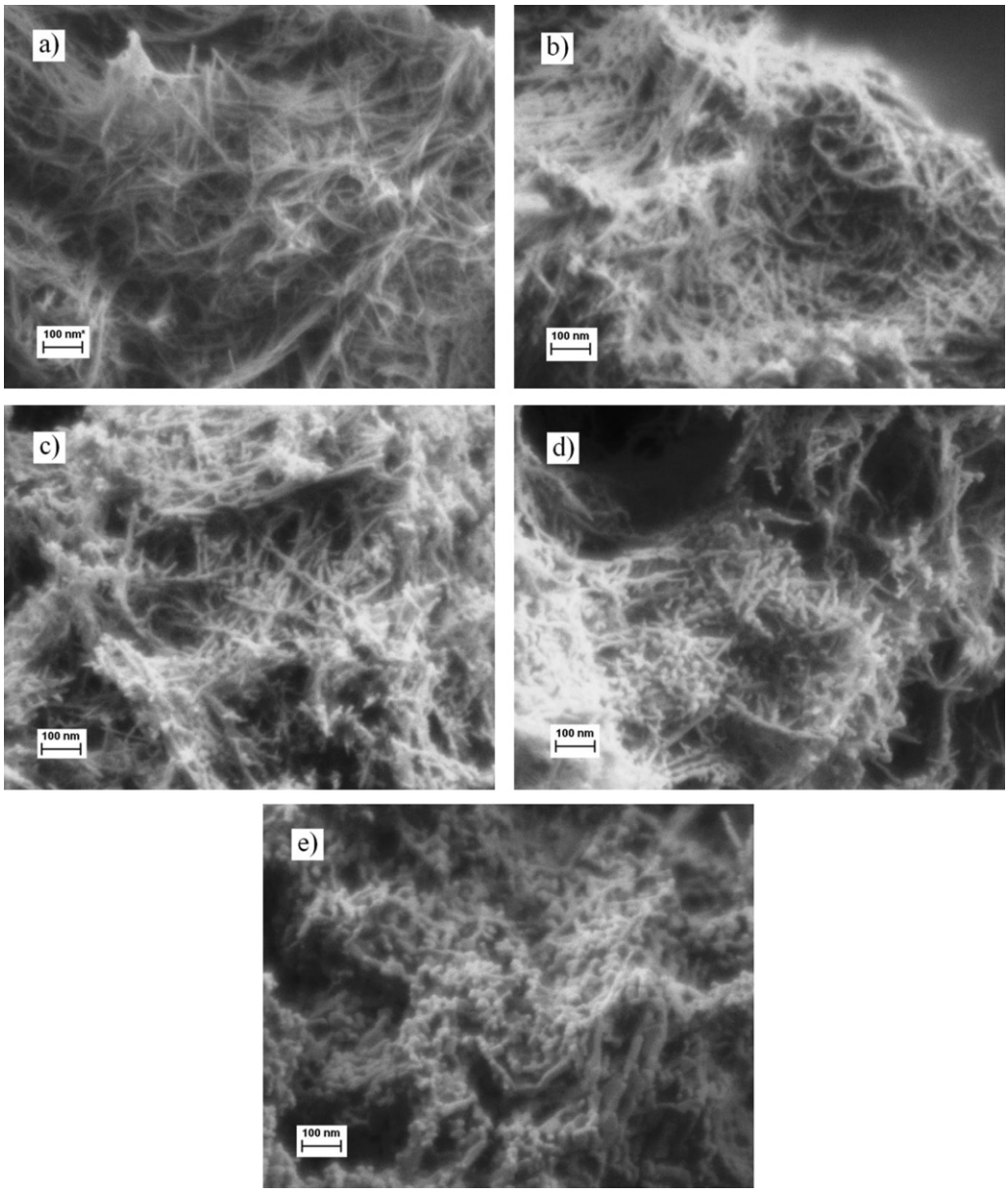

Fig. 2. SEM micrographs of heat-treated protonated titanate nanotubes at (a) 300 °C, (b) 400 °C, (c) 500 °C, (d) 600 °C and (e) 700 °C.

in BET surface area, total pore volume and average pore width are fully consistent with the variation of P25 Degussa powder inputs. Higher initial concentration of starting TiO_2 nanopowder resulted in more homogeneous titanate nanotubes with a decreased size (diameter). These findings can be correlated with results derived from various precipitation procedures, where increased seed concentrations lead to decreased size and homogeneous appearance of precipitates [36]. Therefore, the NT4 sample exhibits the largest BET surface area (highest initial concentration of precursor) among these three samples, while NT5 sample possesses significantly smaller BET surface area (larger particles) as a consequence of decreased starting concentration of TiO_2 powder. The second and the third synthesis (samples NT2 and NT3) were conducted under the same experimental conditions as the first synthesis, except that: (i) 25 bar of inert gas (Ar) was imposed prior the beginning of the hydrothermal experiment (NT2) or (ii) the reaction time was prolonged for another 24 h (sample NT3). Higher pressure in the vessel induced the reaction between TiO_2 (P25 Degussa) and concentrated NaOH towards nanotubular product with enhanced BET surface area, while similar observations were noted also on NT3 sample revealing beneficial impact of reaction time extension.

The synthesis route (Table 1) used for preparation of NT4 sample lead to preferred product, i.e., high surface area and uniform protonated titanate nanotubes obtained in the largest quantity among proposed syntheses. The SEM analysis revealed high equality of nanotubes in NT4 sample (i.e., uniform width of high aspect ratio cylindrical particles), without undesired secondary particles as a consequence of agglomeration of individual morphological forms of titanates into textures, such as nanotubular bundles, split nanofibers, hierarchically linked nanofibers, and so forth. Based on N_2 porosimetry data (Table 3) and thorough analysis of SEM and TEM micrographs, the NT4 sample was selected as a starting material for further preparation of titanate nanotube-based catalysts via heat-treatment at elevated temperatures, which is described in the following chapters.

Scanning and transmission electron microscopy images (Fig. 1) indicate that the alkaline hydrothermal synthesis transformed initial powdered TiO_2 precursor (Fig. 1a) into well developed and

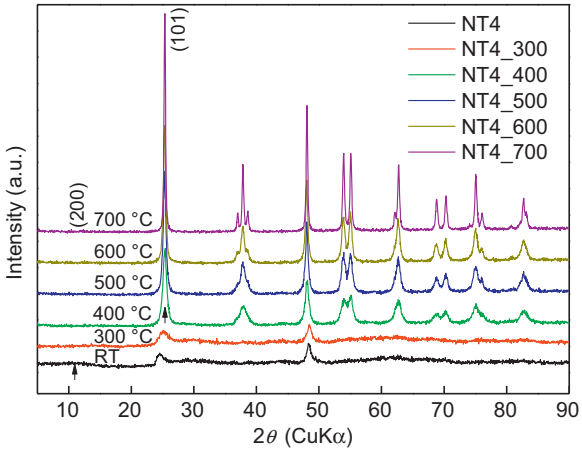

Fig. 3. XRD patterns of the as-prepared protonated titanate nanotubes (NT4) and samples calcined at different temperatures (heat-treatment at 300 °C corresponds to denotation NT4_300, etc).

randomly oriented titanate nanotubes (Fig. 1b and c), which correspond to NT4 synthesis yield. The as-prepared nanotubes are several hundred nanometers in length with the outer diameter of about 10–15 nm. These multiwall structures are actually scrolls of lamellar fragments that are the intermediate phase in the formation process of the titanate nanotubes [37,38]. The exact crystal structure of titanate nanotubes produced by alkaline hydrothermal synthesis is still under debate, however, structures like $Na_xH_{2-x}Ti_3O_7$ and $Na_{2x}H_{2-x}Ti_2O_4(OH)_2$ are usually assigned to titanate nanotubes [39]. Accordingly to the interpretation of obtained XRD data, the $Na_{2x}H_{2-x}Ti_2O_4(OH)_2$ structure (JCPDS, Card 47-0124) gives the best agreement.

3.2. Characterization of titanate nanotube-based catalysts

Nevertheless, such hollow tubular morphology of protonated titanate nanotubes, which can formally be considered as hydrated form of TiO_2, can be transformed into solid nanorods accompanied with surface area decrease and anatase phase appearance when calcined at temperatures above 300 °C [40]. These findings were confirmed by means of SEM microscopy (Fig. 2), BET values and XRD measurements (Fig. 3), which revealed that the heat-treatment at elevated temperatures, ranging from 300 to 700 °C, provoked extensive recrystallization (especially at higher temperatures) noticeable as evident deviance from physicochemical properties of initial nanotubular sample (Fig. 1b and c). An exception among calcined samples can be recognized in the sample prepared at 300 °C, since its morphology resembles the pristine one, confirming that at stated temperature only minute structural changes were induced. As calcination temperature was increased, also the size of newly formed anatase crystals was enlarged as a consequence of rearrangement of building units (octahedral TiO_6), indicating metastability of protonated titanate nanotubes. The driving force for such recrystallization and densification is the change in free energy from the decrease in specific surface area. Moreover, only a very close inspection reveals that the nanotubes (calcined at 400 °C or higher) are actually broken in many places, probably because of mechanical strain during the heating procedure and phase transformation. Such phase transformation and crystal growth is discernible from X-ray diffraction patterns (Fig. 3), demonstrating that only the as-prepared sample and sample NT4_300 (annealed at 300 °C) can be assigned to layered protonated titanate (JCPDS, Card 47-0124) with poor crystallinity [41]. The preserved initial crystal structure of the NT4_300 sample thus confirms the SEM observations (Fig. 2a) regarding heat-unaffected nanotubular

Table 4
Specific surface area (S_{BET}), total pore volume (V_{pore}), average pore width (d_{pore}) and average crystallite size of the as-prepared and heat-treated NT4 samples (catalysts) at temperatures, ranging from 300 to 700 °C.

Sample (catalyst)	S_{BET} ($m^2\ g^{-1}$)	V_{pore} ($cm^3\ g^{-1}$)	d_{pore} (Å)	Crystallite size (Å)
NT4	383	1.41	126	–
NT4_300	348	1.38	133	–
NT4_400	165	1.07	216	108
NT4_500	117	0.68	208	157
NT4_600	95	0.53	201	189
NT4_700	49	0.26	194	359

morphology. The phase transformation is more pronounced already at 400 °C (sample NT4_400) and certainly at higher temperatures. At 400 °C, the layered structure slowly reconstructs into anatase (newly developed diffraction peaks in the NT4_400 XRD spectra), of which crystals grow larger with increasing calcination temperature (higher peak intensities and narrower diffraction peaks). Consequently, at 700 °C (sample NT4_700) the anatase structure is brought to full development and the initial layered structure is ultimately transformed to thermodynamically more stable crystal structure. Narrow Bragg reflections and high peak intensities of NT4_700 sample coincide with SEM image (Fig. 2e), exhibiting large anatase crystallites. The actual anatase crystallite sizes were estimated from the corresponding width of the (1 0 1) diffraction peak ($2\theta = 25.3°$) by Scherrer's formula (see Table 4). As expected, the largest crystallites (35.9 nm) were obtained for the sample that was heat-treated at the highest temperature (i.e., 700 °C) followed by substantially smaller crystallites (18.9 nm), which were determined for the sample annealed at 600 °C. Sample NT4_400 was the last sample containing anatase crystallites (10.8 nm), whereas as mentioned before, the as-prepared and NT4_300 samples were devoid of anatase Bragg reflections.

The dehydration process of the as-prepared protonated titanate nanotubes was analyzed by thermogravimetry (Fig. 4). The TGA plot of NT4 sample shows a weight loss of about 9.5% after heating up to 700 °C in air atmosphere, signifying two distinct dehydration processes: (i) dehydration of intralayered OH groups and (ii) dehydration of interlayered OH groups [40,42]. The weight loss found before 300 °C is usually ascribed to the adsorbed water and intralayered OH groups removal, causing a little modification in nanotube length and (2 0 0) peak intensity. When annealing at temperatures above 300 °C, the dehydration of interlayered OH groups provoked the transition of crystal form from initial protonated titanate to

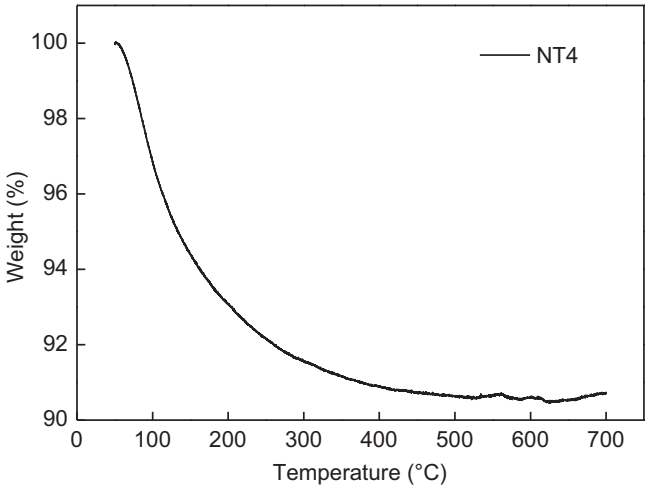

Fig. 4. Thermogravimetric diagram of the as-prepared protonated titanate nanotubes.

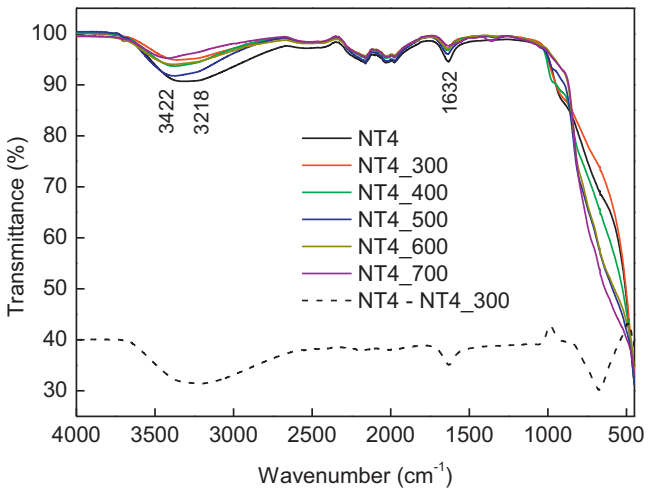

Fig. 5. FT-IR spectra of the as-prepared titanate nanotubes and heat-treated NT4 samples (300–700 °C). The dashed line corresponds to absorption band difference between NT4 and NT4_300 sample.

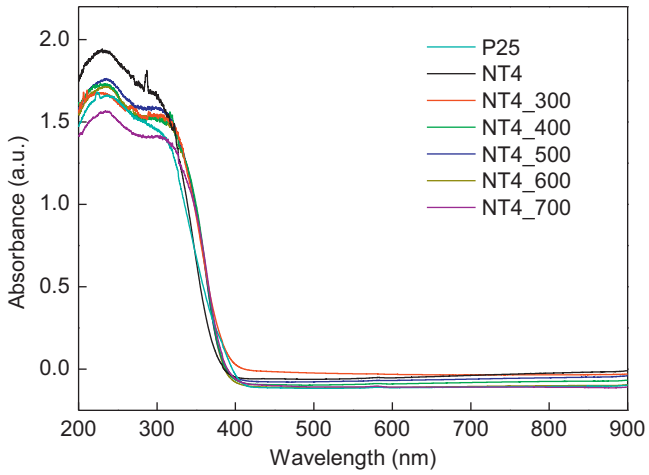

Fig. 6. UV–visible diffuse reflectance spectra of the as-prepared, heat-treated NT4 samples (300–700 °C) and P25 Degussa nanoparticles.

anatase. Such two-step dehydration process, which is finished at about 500 °C, is accompanied by two substantial processes: (i) a phase transformation from layered protonated titanate to anatase and (ii) a morphology transformation from nanotubes to nanorods [40]. Combining the TGA analysis with XRD and SEM observations, it is obvious that layered protonated titanate reconstructs slowly to anatase phase from about 400 °C (the majority of water is already removed). Hereafter (towards 700 °C), the remained water is ultimately eliminated, whereas the anatase phase growth and thus nanotube morphology destruction is without hindrance stimulated in the direction of large, low-surface area anatase particles commonly in agglomerated form.

The abundance of OH groups in protonated titanate nanotubes can also be confirmed by infrared spectroscopy measurements (Fig. 5). The appearance of a characteristic peak at 1632 cm^{-1}, which can be assigned to the H—O—H deformation mode (δ_{H-O-H}), confirms the presence of crystallographic water molecules in the samples. The broad intense band at 3422 cm^{-1} can be attributed to the deformation and stretching vibrations of OH groups of physisorbed water in TiO_2, while the shoulder at 3218 cm^{-1} from Ti—OH bonds was ascribed to the strong interaction between Ti ions and OH groups [43,44]. The dashed curve in Fig. 5 represents the subtracted values of NT4_300 FT-IR spectrum from FT-IR spectrum of the as-prepared titanate nanotubes (NT4), which clarify more intense surface OH stretching mode oscillations and Ti—OH bonds accompanying the uncalcined titanate sample. Namely, during the heat-treatment of NT4_300 sample, surface and crystallographic OH groups were partially eliminated, thus weaker OH absorption bands can be observed from the FT-IR spectrum of NT4_300 sample.

The average particle size is in a good agreement with the BET surface area data (Table 4). The initial BET surface area (383 $m^2\,g^{-1}$) was gradually decreased with the rising calcination temperature, until the final BET surface area of 49 $m^2\,g^{-1}$ was reached (at 700 °C). Similar behaviour was observed with the total pore volume, which was almost three times smaller after calcination at 700 °C (compared to the starting total pore volume), indicating excessive recrystallization and sintering processes. Between 300 and 400 °C, a drastic drop of BET surface area (nearly 200 $m^2\,g^{-1}$) can be noticed as a result of nanotube morphology collapse. In the same temperature range, a considerable increase of average pore size is evident (Table 4) that can be attributed to the loss of small pores within titanate nanotubes. Afterwards, the average pore size was gradually decreasing with increasing temperature of heat treatment due to the enhanced recrystallization of TiO_2. As expected, the pore volume was simultaneously decreasing as a result of persistent material densification. Furthermore, the N_2 adsorption data are undoubtedly reflected in the morphological observations (Fig. 2) and XRD patterns depicted in Fig. 3, thus confirming the above stated explanations of dehydration and consequent phase transformation processes.

The optical behaviour of titanate nanotubes can be studied by measuring their UV–vis absorption, in which the characteristic absorption band of titanate nanotubes should be assigned to the intrinsic transition from the valence band (VB) to the conduction band (CB). Fig. 6 shows the UV–vis diffuse reflectance spectra of various catalysts (pristine NT4 sample, series of heat-treated NT4 samples at different calcination temperatures and reference sample P25 Degussa) prepared in this study. The spectral data of calcined NT4 samples (including NT4_300 sample, which crystal structure is devoid of anatase) exhibit the strong cut off at 381–385 nm; where the absorbance value is minimum. Accordingly, the bang gap energies were calculated to be in the range of 3.23–3.26 eV, which corresponded ideally to the 3.24 eV (cut off at 384 nm) of P25 Degussa sample, approving similar physical properties of the solids, such as electrical resistivity and optical absorption, regardless of the rutile phase presence in P25 Degussa powder (1:4 = rutile:anatase). However, the declinatory behaviour of uncalcined sample (NT4) was witnessed, since the band gap absorption edge was estimated to be shifted deeper into the UV region (373 nm), corresponding to band gap energy of 3.33 eV. The interpretation of the blue-shift is not clear so far. It can be attributed to the larger diameter of protonated titanate nanotubes compared to e.g., NT4_300 sample (nanotubular morphology is still present, but the nanotube diameter is contracted), which is accordingly accountable for the electronic band gap increase [45]. A plausible explanation of the blue-shift in protonated titanate nanotubes can be also recognized in a quantum-size effect [46,47]. Nevertheless, the band gap energy of the uncalcined powder is not significantly different from the other representatives; hence, similar optical properties can be ascribed to the presented group of catalysts.

3.3. CWAO experiments

Preliminary experiments of WAO were performed in order to evaluate BPA hydro-thermal stability at operating conditions (see Table 2; details at 200 °C) used for CWAO. SiC particles (300 mg, average particle diameter of approximately 0.5 mm, BET specific

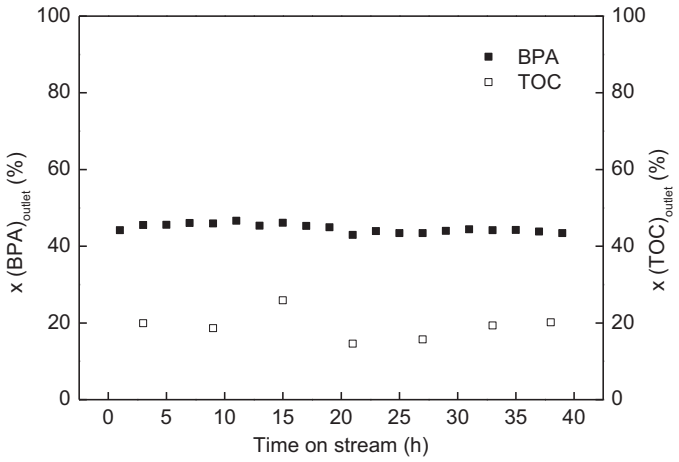

Fig. 7. BPA and TOC conversion as a function of time on stream obtained over SiC at 200 °C. Operating conditions: $p(O_2)$: 10.0 bar, $\Phi_{vol,L}$: 0.5 ml min^{-1}, $c(BPA)_{feed}$: 10.0 mg l^{-1}, T: 200 °C.

surface area below 0.1 m^2 g^{-1}) were used as an inert filler of fixed-bed in a three-phase continuous-flow reactor. Analyses of BPA solutions sampled at the reactor outlet revealed moderate conversions of BPA and adequate TOC conversions (Fig. 7). Since it was verified that the measured BPA conversions were not influenced by adsorption effects, these tests clearly demonstrated the impact of non-catalytic degradation of analyte and confirmed stable operation of the system as a function of time on stream in consecutive WAO runs.

CWAO experiments of model BPA solutions were conducted in the presence of various titanate nanotube-based catalysts (as-prepared protonated titanate nanotubes, series of annealed protonated titanate nanotubes and commercial P25 Degussa). Fig. 8a shows corresponding BPA conversions determined in the end-pipe solutions, indicating significant enhancement in destruction of model aqueous pollutant, if compared to straightforward WAO process performed over inert SiC (Fig. 7). More than two-fold improvement in oxidative BPA destruction was observed with tested catalyst samples. Such enhancement of BPA conversion as a function of time on stream can be attributed to the non-stoichiometric nature of TiO_2 and progressive establishment of gas–liquid–solid equilibrium during the initial stage of CWAO process [48]. After approximately 20 h of time on stream, a steady-state performance was obtained, giving rise to good reproducibility of data. Focused on mature period (after initial non-equilibrium) of BPA removal, it can be perceived that the catalyst annealed at 600 °C (NT4_600) attained the highest BPA conversion among tested titanate nanotube-based catalysts. In general, physicochemical properties of catalysts like crystalline structure, surface area, surface acidity, and surface functional groups are recognized to significantly influence the oxidative reaction efficiency. Among these parameters, a high specific surface area can play a crucial role in certain catalytic reactions, since large adsorption capacity of catalyst usually promotes the reaction rate [49–51]. When compared to the reference TiO_2 powder (P25 Degussa), titanate nanotube-based catalysts exhibit several times larger specific surface area, which makes these materials as promising catalyst candidates. However, according to the BET surface area measurements (Table 4), which demonstrated decreased specific surface area of NT4_600 sample due to heat-treatment induced recrystallization, one can ascertain that extremely high BET surface area of titanate nanotube-based catalysts is not the key parameter for achieving high BPA conversions in CWAO process. Based on these observations, it is evident that other physicochemical properties, such as crystalline

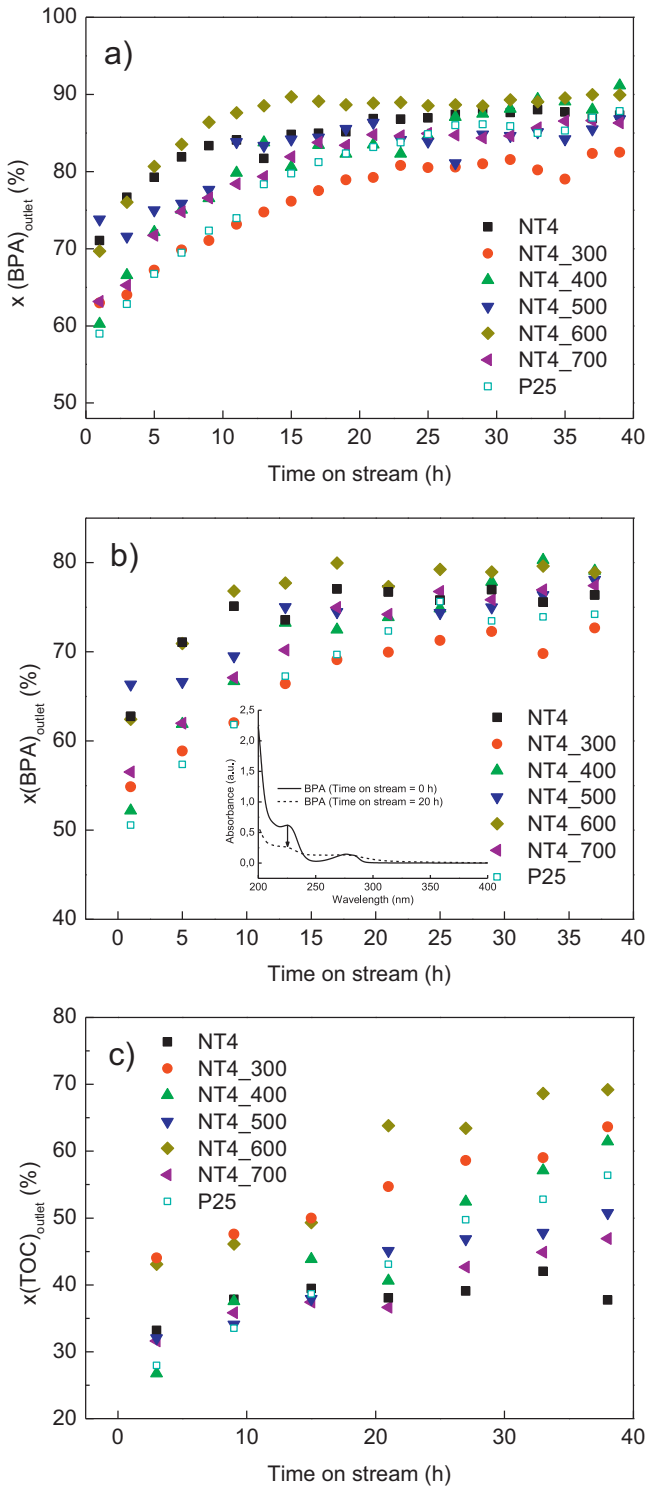

Fig. 8. BPA conversion as a function of time on stream over various titanate nanotube-based catalysts determined by means of (a) HPLC technique and (b) UV–vis spectroscopy, respectively. (c) TOC conversion as a function of time on stream over various titanate nanotube-based catalysts. Operating conditions: $p(O_2)$: 10.0 bar, $\Phi_{vol,L}$: 0.5 ml min^{-1}, $c(BPA)_{feed}$: 10.0 mg l^{-1}, T: 200 °C.

structure, have a more meaningful contribution to the overall catalytic activity. The NT4_600 catalyst exhibits fully transformed anatase structure with crystallite sizes not exceeding 20 nm. On the other hand, the NT4_700 catalyst is constituted of anatase crystallites as well, but showing significantly larger crystallite sizes and

correspondingly decreased BET surface area. The related BPA conversion is noticeable lower in comparison with NT4_600 sample, indicating that balanced physicochemical properties are needed for achieving remarkable conversion rates of BPA aqueous solutions. Hence, as regards the remaining catalysts tested in CWAO process, the BPA conversions were less pronounced, since their specific surface area to crystallinity ratios were not well-adjusted. However, a contradiction arose regarding the as-prepared protonated titanate nanotubes (poor crystallinity), which performed better under CWAO conditions than the few other anatase-based catalysts. A plausible explanation would originate from surface hydroxyl groups, which are abundant on the surface of pristine nanotubular titanates and are characterized by weak Brønsted acidity [52]. A high concentration of —OH groups and strong surface dipole moment could cause hydrophilic properties, which enhanced wettability and thus the effective surface area for oxidative reactions. When annealing at 300 °C or higher, the stripping of the surface —OH groups was pronounced (see Fig. 5), which turned the nanotubular titanates (with poor crystallinity) into less effective catalysts (e.g., NT4_300) for the destruction of aqueous BPA. Eventually, as stated above, the simultaneous emerging of anatase phase with increasing annealing temperature overtook the dominant role in oxidative reaction, which was further stimulated via free-radical mechanism [19].

It can be seen from Fig. 8b that the trend in BPA conversions determined from HPLC spectra (Fig. 8a) is fully consistent with the trend of BPA conversions obtained from UV–vis spectra (analysis of the end-pipe solutions of corresponding BPA oxidation runs). However, the ordinate axis values are shifted towards lower BPA conversions, thus not reaching BPA conversions plotted in Fig. 8a. Such observations are expected, since the UV–vis method is non-selective regarding BPA concentration evaluation; the oxidative reaction by-products absorb the incident beam light at wavelengths characteristic for BPA molecules leading to higher background. As a consequence, the corresponding BPA intensities are higher, while apparent BPA conversions are lower. The insert in Fig. 8b exhibits the UV–vis absorbance spectra of untreated BPA solution (C_{BPA} = 10 mg l^{-1}) and treated BPA solution (after 20 h on stream), which demonstrate weaker absorbance intensities after treatment in CWAO process over annealed titanate nanotubes. Taking into account that BPA conversions derived from UV–vis spectroscopy are inaccurate, this method can still provide supporting and complementary information to precise HPLC measurements.

TOC conversions in end-pipe solutions of corresponding BPA oxidation runs are depicted in Fig. 8c. Again, the trend in TOC conversions is entirely consistent with the trend of BPA conversions derived from HPLC and UV–vis measurements (Fig. 8a and b), respectively. These observations confirm the NT4_600 powder as the most efficient titanate nanotube-based catalyst for mineralization of model aqueous organic compound. When the initial non-equilibrium operating conditions were overcome, up to 70% of initial BPA could be mineralized into CO_2 and H_2O. Based on complementary IC and HPLC analyses of treated liquid-phase samples, the residual organic content could be attributed to the presence of non-oxidized and refractory short-chain carboxylic acids (mainly acetic and formic acid). A typical concentration determined for acetic and formic acid (e.g., sample treated over NT4_700) was 1.13 and 0.52 ppm, respectively. However, these results are not surprising for active metal-free catalysts, since many studies have shown that low molecular-weight carboxylic acids are refractory to be ultimately oxidized into CO_2 and H_2O [27].

In the WAO/CWAO of organic compounds, the reaction temperature is a key parameter influencing the removal of aqueous pollutants. Generally, at higher operating temperatures, higher pollutant conversions and reaction rates are obtained [25]. Furthermore, the increased height of fixed-bed (higher catalyst loading) additionally promotes higher reactant conversion, because of prolongation of the residence time. The effect of higher catalyst loading, i.e., 500 mg of NT4_600 catalyst (as the most efficient representative), is clearly visible in Fig. 9a, where BPA conversion as a function of time on stream is depicted. Focused on the first period of CWAO experiment, which was performed at 200 °C, one can ascertain that BPA destruction was significantly improved as compared to the runs conducted over lower catalyst loading (Fig. 8a). Under newly set experimental conditions, BPA conversions up to 98% were achieved (after reaching the dynamic equilibrium). It can be seen that with increasing temperature further to 210 °C, total conversion of BPA was attained (focused on subsequent oxidation runs after 47 h on stream). These results clearly demonstrate a stable oxidative reaction over noble metal-free, heat-treated titanate nanotubes, with no discernible catalyst deactivation even after considerable long period on stream.

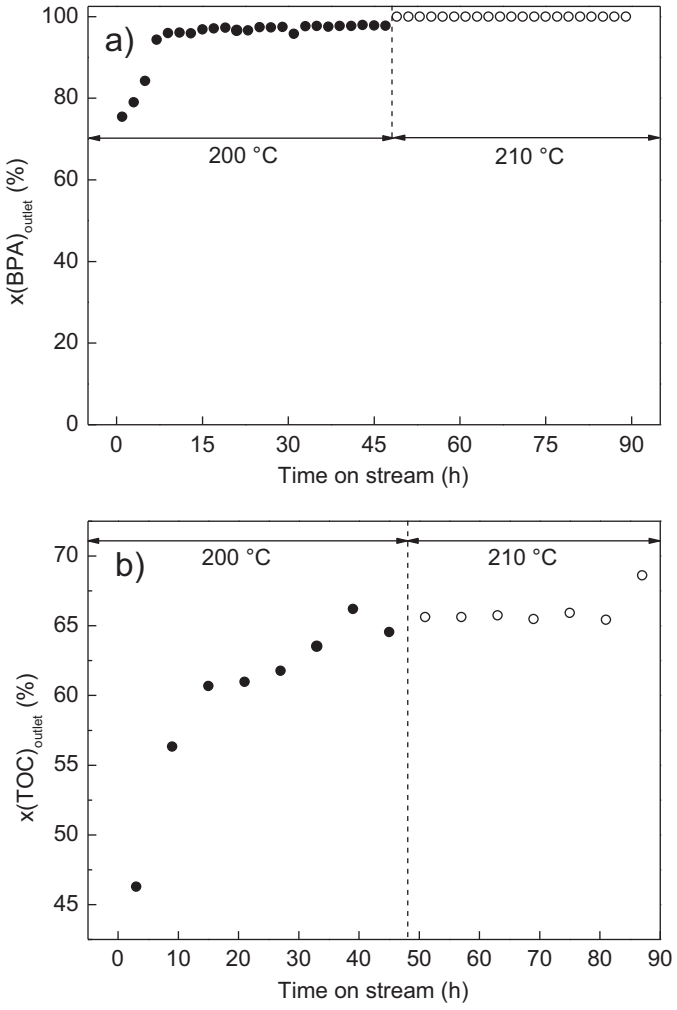

Fig. 9. (a) BPA and (b) TOC conversion as a function of time on stream measured during consecutive BPA oxidation at two dissimilar reaction temperatures over 500 mg of NT4_600 catalyst. Operating conditions: $p(O_2)$: 10.0 bar, $\Phi_{vol,L}$: 0.5 ml min^{-1}, $c(BPA)_{feed}$: 10.0 mg l^{-1}.

Simultaneously, TOC removal was monitored (Fig. 9b) under the same operating conditions as described in the previous paragraph referring to BPA conversion over 500 mg of NT4_600 catalyst. Interestingly, the extent of BPA mineralization was comparable to TOC conversions obtained under milder operation conditions (Fig. 8c), indicating that for efficient removal of resistant intermediates (e.g., carboxylic acids): (i) even harsher experimental conditions should

Table 5
Carbon content (measured by means of CHNS elemental analysis) on the surface of fresh and spent catalyst samples used in the CWAO process of BPA, and TOC conversions combined with TOC percentages deposited on the catalyst surface. Operating conditions: $p(O_2)$: 10.0 bar, $\Phi_{vol,L}$: 0.5 ml min^{-1}, $c(BPA)_{feed}$: 10.0 mg l^{-1}, T: 200 °C.

Sample	TOC (%) removal	TC (mg g^{-1}) fresh	TC (mg g^{-1}) spent	TOC (%) accumulated
NT4	42	6.5	3.3	–
NT4_300	64	3.4	3.3	–
NT4_400	61	2.5	3.2	3.6
NT4_500	58	1.9	2.8	4.9
NT4_600	69	1.7	1.9	0.9
NT4_700	47	1.5	2.7	8.0
P25 Degussa	56	0.4	2.7	12.9

be set, (ii) residence time of the liquid phase should be prolonged, or (iii) a noble metal-supported catalyst should be used.

Finally, no leaching of titanium (to the detection limit of 0.01 mg l^{-1}) was detected by IC-AES analysis in the end-pipe liquid-phase samples of CWAO experiments performed in the presence of solids examined in this study.

3.4. Carbon analysis of catalysts

In order to evaluate the amount of accumulated carbonaceous deposits on the catalyst surface, the CHNS analysis of fresh and spent catalysts (after reaction under oxidative conditions) was performed (Table 5). Rather high carbon content was characteristic for fresh catalysts examined in the study, which could be attributed to the high specific surface area available for accumulation of carbonaceous molecules (e.g., CO_2). Accordingly, the TC values of fresh catalysts were getting smaller as the annealing temperature of catalysts was increasing, which in a majority eliminated the initial carbonaceous deposits. Interestingly, the TC values of spent catalysts were insignificant; the reaction of BPA oxidation over NT4 and NT4_300 samples even partially removed the surface carbon deposits, respectively. It is apparent from these observations that the TOC conversions depicted in Fig. 8c and listed in Table 5 correspond to the actual transformations of BPA into reaction products, meaning that negligible portion of the total organic carbon was truly accumulated on the surface of solids during the CWAO of BPA. The exact percentages of accumulated TOC are exhibited in Table 5 as well. Once more, owing to the TC deficit regarding NT4 and NT4_300 catalysts, TOC accumulations were not calculated, while the rest of prepared powders revealed sustainable low TOC deposits, ranging from 0.9 to 8.0%. Interestingly, these TOC values were remarkably lower compared to TOC accumulation portion of P25 Degussa sample. Inversely proportional to BPA conversions over NT4_600 sample (Fig. 8a), which were the highest among tested catalysts, the accumulation of TOC on NT4_600 catalyst surface (0.9%) was the lowest in comparison with other solids, giving another proof of the most balanced physicochemical properties among presented catalysts. Therefore, the synthesized catalysts based on protonated titanate nanotubes represent promising catalyst candidates for a long-term catalytic wet air oxidation of emerging refractory pollutants.

4. Conclusions

To sum up, various catalysts on the basis of titanate nanotubes were prepared by means of alkaline hydrothermal synthesis and subsequent heat-treatment at temperatures ranging from 300 to 700 °C. In the first step, different hydrothermal synthesis conditions were varied in order to obtain copious and uniform high aspect ratio nanotubular solids. The selected material was then further developed by annealing, with intention of varying the crystal structure, specific surface area, and other physicochemical properties, which could significantly contribute to the total catalytic activity. These bare (active metal-free) titanate nanotube-based solids were subjected to catalytic wet air oxidation process of BPA as a representative of emerging organic compound exhibiting estrogenicity. The CWAO experiments were conducted in a continuous-flow trickle-bed reactor at temperatures up to 210 °C and oxygen partial pressure of 10.0 bar. In the presence of NT4_600 (heat-treated at 600 °C) catalyst, the most efficient destruction of BPA was observed among inspected catalysts. Namely, at incentive reaction conditions (210 °C and catalyst loading of 0.5 g) complete BPA removal was achieved. Corresponding TOC removal reached 70%, indicating the presence of non-oxidized, refractory short-chain carboxylic acids, which was confirmed by IC analytical technique. In general, an anatase crystal structure and specific surface area played a crucial role in extent of catalytic oxidation of BPA molecules via oxygen activation mechanism. On the other hand, the as-prepared (non-calcined) sample with the abundance of surface OH groups and undeveloped anatase phase showed an alternative route to destruct water dissolved BPA molecules. CHNS analysis of fresh and spent solids confirmed that negligible amounts of carbonaceous deposits were accumulated on the catalyst surface during the CWAO runs. Since no catalyst deactivation occurred and significant BPA conversions were obtained, the titanate-based nanotubes could be regarded as promising heterogeneous catalysts for degradation of hazardous organic compounds without concern over environmental risk due to active metal leaching from the reactor system and high initial investments (avoiding of noble metals).

Acknowledgements

The authors gratefully acknowledge the financial support of the Ministry of Education, Science, Culture and Sport of the Republic of Slovenia through Research program P2-0150.

References

[1] C.A. Staples, P.B. Dom, G.M. Klecka, S.T. O'Blook, L.R. Harris, Chemosphere 36 (1998) 2149.
[2] M. Fürhacker, S. Scharf, H. Weber, Chemosphere 41 (2000) 751.
[3] H.M. Kuch, K. Ballschmiter, Environmental Science and Technology 35 (2001) 3201.
[4] R. Wang, R. Ren, S. Xia, Y. Zhang, J. Zhao, Journal of Hazardous Materials 169 (2009) 926.
[5] J.H. Kang, D. Aasi, Y. Katayama, Critical Reviews in Toxicology 37 (2007) 607.
[6] P. Preziosi, Pure and Applied Chemistry 70 (1998) 1617.
[7] J. Hoigue, H. Bader, W.R. Haag, J. Taehein, Water Research 19 (1985) 993.
[8] J. Spivack, T.K. Leib, J.H. Lobos, Journal of Biological Chemistry 269 (1994) 7323.
[9] S.K. Marttinen, R.H. Kettunen, J.A. Rintala, Science of the Total Environment 301 (2003) 1.
[10] M. Clara, B. Strenn, E. Saracevic, N. Kreuzinger, Chemosphere 56 (2004) 843.
[11] S.C. Wilson, R.E. Alcock, A.P. Sewart, K.C. Jones, Journal of Environmental Quality 26 (1997) 1467.
[12] J. Zhao, Y. Li, C. Zhang, Q. Zeng, Q. Zhou, Journal of Hazardous Materials 155 (2008) 305.
[13] G.M. Klecka, S.J. Gonsior, R.J. West, P.A. Goodwin, D.A. Markham, Environmental Toxicology and Chemistry 20 (2001) 2725.
[14] Y.-T. Xie, H.-B. Li, L. Wang, Q. Liu, Y. Shi, H.-Y. Zheng, M. Zhang, Y.-T. Wu, B. Lu, Water Research 45 (2011) 1189.
[15] R.A. Torres, C. Petrier, E. Combet, M. Carrier, C. Pulgarin, Ultrasonics Sonochemistry 15 (2008) 605.
[16] Y. Ohko, S. Ando, C. Niwa, T. Tatsuma, T. Yamamura, T. Nakashima, Y. Kubota, A. Fujishima, Environmental Science and Technology 35 (2001) 2365.

[17] M. Deborde, S. Rabouan, P. Mazellier, J.P. Duguet, B. Legube, Water Research 42 (2008) 4299.
[18] I. Iordache, S. Wilson, E. Lundanes, N. Aelenei, Journal of Hazardous Materials 142 (2007) 559.
[19] M. Bistan, T. Tišler, A. Pintar, Catalysis Communications 22 (2012) 74.
[20] J. Levec, A. Pintar, Catalysis Today 124 (2007) 172.
[21] K.H. Kim, S.K. Ihm, Journal of Hazardous Materials 186 (2011) 16.
[22] L. Oliviero, J. Barbier, D. Duprez, Applied Catalysis B: Environmental 40 (2003) 163.
[23] F. Luck, Catalysis Today 53 (1999) 81.
[24] S. Roy, M. Vashishtha, A.K. Saroha, Journal of Engineering Science and Technology Review 3 (1) (2010) 95.
[25] A. Pintar, J. Batista, T. Tišler, Applied Catalysis B: Environmental 84 (2008) 30.
[26] S. Yang, W. Zhu, J. Wang, Z. Chen, Journal of Hazardous Materials 153 (2008) 1248.
[27] S. Yang, W. Zhu, Z. Jiang, Z. Chen, J. Wang, Applied Surface Science 252 (2006) 8499.
[28] L.S. Wang, M.W. Xiao, X.J. Huang, Y.D. Wu, Journal of Hazardous Materials 161 (2009) 49.
[29] D.V. Bavykin, J.M. Friedrich, F.C. Walsh, Advanced Materials 18 (2006) 2807.
[30] P. Hoyer, Langmuir 12 (1996) 1411.
[31] D. Gong, C.A. Grimes, O.K. Varghese, W. Hu, R.S. Singh, Z. Chen, E.C. Dickey, Journal of Materials Research 16 (2001) 3331.
[32] T. Kasuga, M. Hiramatsu, A. Hoson, T. Sekino, K. Niihara, Advanced Materials 11 (1999) 1307.
[33] S. Kim, M. Kim, S.H. Hwang, S.K. Lim, Applied Catalysis B: Environmental 123–124 (2012) 391.
[34] J. Jamnik, R. Dominko, B. Erjavec, M. Remškar, A. Pintar, M. Gaberšček, Advanced Materials 21 (2009) 2715.
[35] C.C. Tsai, H. Teng, Chemistry of Materials 18 (2006) 367.
[36] S. Sathyamoorthy, G.D. Moggridge, M.J. Hounslow, Crystal Growth and Design 1 (2001) 123.
[37] P. Umek, P. Cevc, A. Jesih, A. Gloter, C.P. Ewels, D. Arčon, Chemistry of Materials 17 (2005) 5945.
[38] S. Ribbens, V. Meynen, G.V. Tendeloo, X. Ke, M. Mertens, B.U.W. Maes, P. Cool, E.F. Vansant, Microporous and Mesoporous Materials 114 (2008) 401.
[39] H.H. Ou, S.L. Lo, Separation and Purification Methods 58 (2008) 179.
[40] H. Zhang, G.R. Li, L.P. An, T.Y. Yan, X.P. Gao, H.Y. Zhu, Journal of Physical Chemistry C 111 (2007) 6143.
[41] J. Yang, Z. Jin, X. Wang, W. Li, J. Zhang, S. Zhang, X. Guo, Z. Zhang, Dalton Transactions (2003) 3898.
[42] M. Zhang, Z. Jin, J. Zhang, X. Guo, J. Yang, W. Li, X. Wang, Z. Zhang, Journal of Molecular Catalysis 217 (2004) 203.
[43] M.L. Qian, T. Zhang, S. Wageh, Z.S. Jin, Z.L. Du, Y.S. Wang, X.R. Xu, Nanotechnology 17 (2006) 100.
[44] W. Wang, J. Zhang, H. Huang, Z. Wu, Z. Zhang, Colloids and Surfaces A 317 (2008) 270.
[45] Z. Liu, Q. Zhang, L.C. Qin, Solid State Communications 141 (2007) 168.
[46] G.K. Mor, O.K. Varghese, M. Paulose, K. Shankar, C.A. Grimes, Solar Energy Materials and Solar Cells 90 (2006) 2011.
[47] T. Takagahara, K. Takeda, Physical Review B 46 (1992) 15578.
[48] A. Bielanski, J. Haber, Oxygen in Catalysis, M. Dekker, New York, 1991.
[49] K.H. Wang, Y.H. Hsieh, C.H. Wu, C.Y. Chang, Chemosphere 40 (2000) 389.
[50] Y. Chen, K. Wang, L. Lou, Journal of Photochemistry and Photobiology A 163 (2004) 281.
[51] D.W. Bahnemann, S.N. Kholuiskaya, R. Dillert, A.I. Kulak, A.I. Kokorin, Applied Catalysis B: Environmental 36 (2002) 161.
[52] D.V. Bavykin, F.C. Walsh, Titanate and Titania Nanotubes, RCS, Cambridge, 2010.